Dilute Fermi gas at fourth order in effective field theory

C. Wellenhofer,[1, 2, *] C. Drischler,[3, 4, †] and A. Schwenk[1, 2, 5, ‡]

[1]*Institut für Kernphysik, Technische Universität Darmstadt, 64289 Darmstadt, Germany*
[2]*ExtreMe Matter Institute EMMI, GSI Helmholtzzentrum für Schwerionenforschung GmbH, 64291 Darmstadt, Germany*
[3]*Department of Physics, University of California, Berkeley, CA 94720*
[4]*Lawrence Berkeley National Laboratory, Berkeley, CA 94720*
[5]*Max-Planck-Institut für Kernphysik, Saupfercheckweg 1, 69117 Heidelberg, Germany*

Using effective field theory methods, we calculate for the first time the complete fourth-order term in the Fermi-momentum or $k_\mathrm{F} a_s$ expansion for the ground-state energy of a dilute Fermi gas. The renormalization of the logarithmic divergences that give rise to the nonanalytic part of the fourth-order term is discussed in detail. The convergence behavior of the expansion is examined for the case of spin one-half fermions and compared against quantum Monte-Carlo results, showing that the Fermi-momentum expansion is well-converged at this order for $|k_\mathrm{F} a_s| \lesssim 0.5$.

The dilute Fermi gas has been a central problem for many-body calculations for decades [1–8]. Renewed interest in this problem has been triggered by striking progress with ultracold atomic gases. On the theoretical side, a systematic approach towards the dynamics of fermions (or bosons) at low energies has emerged in the form of effective field theory (EFT) [9–14]. Motivated by this, we revisit the expansion in the Fermi momentum k_F of the ground-state energy density $E(k_\mathrm{F})$ of a dilute gas of interacting fermions. Using perturbative EFT methods, we calculate $E(k_\mathrm{F})$ up to fourth order in the expansion, including for the first time the complete fourth-order term. As we show, our results provide high-order benchmarks regarding the convergence behavior of the expansion, and allow to predict $E(k_\mathrm{F})$ including systematic uncertainty estimates.

Short-ranged EFT represents a general framework for the dynamics of fermions (or bosons) at low momenta $Q < \Lambda_b$, where Λ_b denotes the breakdown scale. The EFT Lagrangian is given by the most general operators consistent with Galilean invariance, parity, and time-reversal invariance. Assuming spin-independent interactions, the (unrenormalized) Lagrangian reads (see, e.g., Refs. [9–14])

$$\mathscr{L}_{\mathrm{EFT}} = \psi^\dagger \left[i\partial_t + \frac{\overrightarrow{\nabla}^2}{2M} \right] \psi - \frac{C_0}{2}(\psi^\dagger \psi)^2$$
$$+ \frac{C_2}{16} \left[(\psi\psi)^\dagger (\psi \overleftrightarrow{\nabla}^2 \psi) + \mathrm{h.c.} \right]$$
$$+ \frac{C_2'}{8} (\psi \overleftrightarrow{\nabla} \psi)^\dagger \cdot (\psi \overleftrightarrow{\nabla} \psi) - \frac{D_0}{6}(\psi^\dagger \psi)^3 + \dots, \quad (1)$$

where ψ are nonrelativistic fermion fields, $\overleftrightarrow{\nabla} = \overleftarrow{\nabla} - \overrightarrow{\nabla}$ is the Galilean invariant derivative, h.c. the Hermitian conjugate, and M the fermion mass. For natural systems the interaction terms of $\mathscr{L}_{\mathrm{EFT}}$ are ordered in powers of fields and derivatives (and suppressed with respect to the kinetic term), so in this case low-energy observables can be calculated systematically by ordering the various contributions in perturbation theory with respect to powers of Q/Λ_b.

The ultraviolet (UV) divergences that appear beyond tree level in perturbation theory can be regularized by introducing a momentum cutoff Λ. By Galilean invariance, the cutoff must be attached to relative momenta $\mathbf{p}^{(\prime)}$ and Jacobi momenta $\mathbf{q}^{(\prime)}$, respectively. The two- and three-body potentials emerging from $\mathscr{L}_{\mathrm{EFT}}$ are then given by

$$\langle \mathbf{p}' | V_{\mathrm{EFT}}^{(2)} | \mathbf{p} \rangle = \Big[C_0(\Lambda) + C_2(\Lambda)(\mathbf{p}'^2 + \mathbf{p}^2)/2$$
$$+ C_2'(\Lambda)\, \mathbf{p}' \cdot \mathbf{p} + \dots \Big]$$
$$\times \theta(\Lambda - p)\theta(\Lambda - p'), \quad (2)$$
$$\langle \mathbf{p}'\mathbf{q}' | V_{\mathrm{EFT}}^{(3)} | \mathbf{p}\mathbf{q} \rangle = \Big[D_0(\Lambda) + \dots \Big] \times \theta(\Lambda - p)\theta(\Lambda - q)$$
$$\times \theta(\Lambda - p')\theta(\Lambda - q'). \quad (3)$$

Perturbative renormalization is carried out by introducing counterterms such that the divergent contributions are cancelled. In the two-body sector, this leads to

$$C_0(\Lambda) = C_0 + C_0 \sum_{\nu=1}^{3} \left(C_0 \frac{M}{2\pi^2} \Lambda \right)^\nu + C_2 C_0 \frac{M}{3\pi^2}\Lambda^3 + \dots, \quad (4)$$

$$C_2(\Lambda) = C_2 + C_2 C_0 \frac{M}{\pi^2} \Lambda + \dots, \quad (5)$$

$$C_2'(\Lambda) = C_2' + \dots, \quad (6)$$

where the cutoff-dependent parts are counterterms. In the natural case the low-energy constants C_0, C_2, and C_2' scale according to

$$C_0 \sim \frac{1}{M\Lambda_b}, \qquad C_2 \sim C_2' \sim \frac{1}{M\Lambda_b^3}. \quad (7)$$

For the renormalized two-body potential the residual cutoff dependence due to terms $\mathcal{O}(1/\Lambda)$ in perturbation theory vanishes in the limit $\Lambda \to \infty$. Matching the two-body low-energy constants to the effective-range expansion (ERE) then leads to (see, e.g., Ref. [10])

$$C_0 = \frac{4\pi a_s}{M}, \qquad C_2 = C_0 \frac{a_s r_s}{2}, \qquad C_2' = \frac{4\pi a_p^3}{M}, \quad (8)$$

where a_s and a_p is the S- and P-wave scattering length, respectively, and r_s is the S-wave effective range.

In the two-body sector there are only power divergences, but in systems with more than two particles also logarithmic divergences can occur, starting at order $(Q/\Lambda_b)^4$. The counterterm for the leading logarithmic divergences is provided by the leading term of the three-body potential $V_{\mathrm{EFT}}^{(3)}$. Neglecting $\mathcal{O}(1/\Lambda)$ terms, cutoff independence in the N-body sector with $N \geqslant 3$ at order $(Q/\Lambda_b)^4$ is tantamount to

$$\frac{\partial}{\partial \Lambda} \left[-(C_0)^4 \beta \ln \Lambda + D_0(\Lambda) \right] = 0. \tag{9}$$

The coefficient of the $\ln \Lambda$ term in Eq. (9) is $\beta = M^3(4\pi^2 - 3\sqrt{3})/(4\pi^3)$, which can be obtained from the UV analysis of the two logarithmically divergent three-body scattering diagrams at order $(Q/\Lambda_b)^4$, see Refs. [4, 10, 15]. Integrating Eq. (9) leads to

$$D_0(\Lambda) = D_0(\Lambda_0) + (C_0)^4 \beta \ln(\Lambda/\Lambda_0). \tag{10}$$

The parameter $D_0(\Lambda_0)$ has to be fixed by matching to few-body data. For $\Lambda_0 \sim Q$ it is $D_0(\Lambda_0) \sim 1/(M\Lambda_b^4)$ in the natural case. The scale Λ_0 is however completely arbitrary: from Eq. (9), $D_0(\Lambda_0)$ scales according to $D_0(\Lambda_0') = D_0(\Lambda_0) + (C_0)^4 \beta \ln(\Lambda_0'/\Lambda_0)$, therefore $V_{\mathrm{EFT}}^{(3)}$ is independent of Λ_0.

Applying the EFT potential $V_{\mathrm{EFT}} = V_{\mathrm{EFT}}^{(2)} + V_{\mathrm{EFT}}^{(3)}$ in many-body perturbation theory (MBPT) leads to the Fermi-momentum expansion for the ground-state energy density $E(k_{\mathrm{F}})$ of the dilute Fermi gas, i.e.,

$$E(k_{\mathrm{F}}) = n \frac{k_{\mathrm{F}}^2}{2M} \left[\frac{3}{5} + (g-1) \sum_{n=1}^{\infty} \mathcal{C}_n(k_{\mathrm{F}}) \right], \tag{11}$$

where $n = g\, k_{\mathrm{F}}^3/(6\pi^2)$ is the fermion number density and g is the spin multiplicity. The dependence of a given MBPT diagram on g is obtained by inserting a factor $\delta_{\sigma_1,\sigma_1'}\delta_{\sigma_2,\sigma_2'} - \delta_{\sigma_1,\sigma_2'}\delta_{\sigma_2,\sigma_1'}$ for each vertex and summing over the spins $\sigma_1^{(\prime)}$, $\sigma_2^{(\prime)}$ of the in- and outgoing lines.

The three leading terms in the expansion are given by [1, 3, 5–8, 10, 16, 17]

$$\mathcal{C}_1(k_{\mathrm{F}}) = \frac{2}{3\pi} k_{\mathrm{F}} a_s, \tag{12}$$

$$\mathcal{C}_2(k_{\mathrm{F}}) = \frac{4}{35\pi^2}(11 - 2\ln 2)(k_{\mathrm{F}} a_s)^2, \tag{13}$$

$$\mathcal{C}_3(k_{\mathrm{F}}) = \left[0.0755732(0) + 0.0573879(0)\,(g-3) \right](k_{\mathrm{F}} a_s)^3$$
$$+ \frac{1}{10\pi}(k_{\mathrm{F}} a_s)^2 k_{\mathrm{F}} r_s + \frac{1}{5\pi}\frac{g+1}{g-1}(k_{\mathrm{F}} a_p)^3. \tag{14}$$

The numerical values in the expression for $\mathcal{C}_3(k_{\mathrm{F}})$ are the ones obtained by Kaiser [16, 17] using semianalytic methods. We have reproduced these results. Our result

for the fourth-order term is given by

$$\mathcal{C}_4(k_{\mathrm{F}}) = -0.0425(1)\,(k_{\mathrm{F}} a_s)^4 + 0.0644872(0)\,(k_{\mathrm{F}} a_s)^3 k_{\mathrm{F}} r_s$$
$$+ \gamma_4\,(g-2)\,(k_{\mathrm{F}} a_s)^4, \tag{15}$$

with

$$\gamma_4(k_{\mathrm{F}}) = \frac{M D_0(\Lambda_0)}{108\pi^4 a_s^4} + 0.2707(4) - 0.00864(2)\,(g-2)$$
$$+ \frac{16}{27\pi^3}\left(4\pi - 3\sqrt{3} \right) \ln(k_{\mathrm{F}}/\Lambda_0). \tag{16}$$

Here, the effective-range contribution stems from the two second-order diagrams with one C_0 and one C_2 vertex (plus the corresponding tree-level counterterm), which can be evaluated using the semianalytic formula of Kaiser [18]. The remaining part of $\mathcal{C}_4(k_{\mathrm{F}})$ corresponds to diagrams with four C_0 vertices and the tree-level contribution from $V_{\mathrm{EFT}}^{(3)}$.

Setting $\Lambda_0 = 1/|a_s|$ one obtains from the nonanalytic part of $\gamma_4(k_{\mathrm{F}})$ the known form of the logarithmic term at fourth order [2, 4, 6, 7, 10]. Note again that Λ_0 is an arbitrary auxiliary scale: from Eq. (9), $\gamma_4(k_{\mathrm{F}})$ is independent of Λ_0. Therefore, the logarithmic term at fourth order should not be treated as a separate contribution in the k_{F} expansion.

For a momentum-independent potential (i.e., for the $C_0(\Lambda)$ part of $V_{\mathrm{EFT}}^{(2)}$), only diagrams without single-vertex loops contribute at zero temperature. There are 39 such diagrams at fourth order in MBPT [6, 19], which can be divided into four topological species:

- I(1-6): ladder diagrams,

- IA(1-3): ring diagrams,

- II(1-12), IIA(1-6): other two-particle irreducible diagrams,

- III(1-12): two-particle reducible diagrams.

Here, we have followed Baker's [6] convention for the labeling of these diagrams according to groups that are closed under vertex permutations. Diagrams III(3,6,11,12) are anomalous and thus give no contribution in zero-temperature MBPT [20]. The remaining diagrams are listed in Table 1. The diagrams in the pairs I(3,4), III(7,8) and III(9,10) can be combined to get simplified energy denominators; I(2,5), II(1,2), II(3,4), II(7,8), II(11,12) and IIA(2,4) give identical results for a spin-independent potential; and for a momentum-independent potential the contribution from I(3+4) is half of that from I(2+5).

The diagrams I(1-6) can be calculated using the semianalytic expressions derived by Kaiser [16], which can be obtained from the usual MBPT expressions [19] by applying various partial-fraction decompositions and the Poincaré-Bertrand transformation formula [21].

Table I. Results for the regular contributions to $\mathcal{C}_4(k_{\mathrm{F}})$. Diagrams with * (**) have UV power (logarithmic) divergences, which are subtracted by the respective counterterm contributions. Diagrams with *** have infrared singularities. The uncertainty estimates take into account both the statistical Monte-Carlo uncertainties and variations of the (numerical) cutoff. The g factors are listed without the generic $g(g-1)$ factor.

diagram	g factor	value
I1*	1	$+0.0383115(0)$
I2*+I3+I4*+I5*	1	$+0.0148549(0)$
I6	1	$-0.0006851(0)$
IA1	$g(g-3)+4$	$-0.003623(1)$
IA2	$g(g-3)+4$	$-0.001672(1)$
IA3	$g(g-3)+4$	$-0.003343(1)$
II1*+II2*	$g-3$	$+0.058359(1)$
II3+II4	$g-3$	$-0.003358(1)$
II5**	$g-3$	$+0.0645(1)$
II6**,*	$g-3$	$-0.0265(2)$
II7+II12	$g-3$	$+0.003923(1)$
II8+II11	$g-3$	$+0.007667(1)$
II9	$g-3$	$-0.000981(1)$
II10	$g-3$	$-0.000347(1)$
IIA1**	$3g-5$	$+0.0647(1)$
IIA2+IIA4	$3g-5$	$+0.004122(1)$
IIA3	$3g-5$	$-0.000461(1)$
IIA5	$3g-5$	$+0.003542(1)$
IIA6	$3g-5$	$+0.003331(1)$
III1***,**,*+III7+III8***,*	$g-1$	$-0.0513(2)$
III2***+III9+III10***	$g-1$	$+0.001650(1)$
(II5+IIA1)$_{g=2}$	1	$+0.00018(1)$
(II6+III1+III7+III8)$^*_{g=2}$	1	$-0.0248(1)$
$\sum_{\mathrm{diagrams},g=2}$	1	$-0.0425(1)$

For the numerical evaluation of the IA diagrams it is more convenient to use single-particle momenta instead of relative momenta, because then the phase space is less complicated. We have carried out the numerical calculations using the Monte-Carlo framework introduced in Ref. [22] to evaluate high-order many-body diagrams.

The II, IIA and III diagrams without divergences can be evaluated in the same way as the IA diagrams. The following diagrams involve divergences:

- I(1,2,4,5), II(1,2,6), III(1,8): UV power divergences,

- II(5,6), IIA1, III1: logarithmic UV divergences,

- III(1,2,8,10): infrared divergences.

The UV power divergences correspond to particle-particle ladders and are cancelled by counterterm contributions from the the first-, second-, and third-order diagrams obtained by removing the ladders. The diagrams with logarithmic divergences II(5,6), IIA1 and III1 are shown in Fig. 1. Using dimensionless momenta $\mathbf{i} \equiv \mathbf{k}_i/(\alpha k_{\mathrm{F}})$ one can analytically extract (in
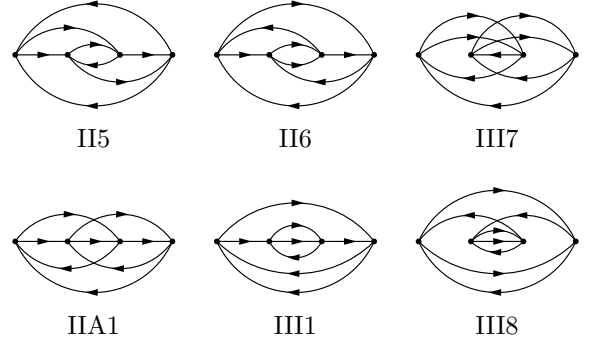

Figure 1. Hugenholtz diagrams representing the fourth-order contributions with logarithmic divergences II(5,6), IIA1, and III1. Also shown are the other diagrams that are part of the sum III(1+7+8).

the limit $\Lambda \to \infty$) from each diagram a contribution $\sim \ln(\Lambda/(\alpha k_{\mathrm{F}}))$. The parameter α is arbitrary, and can be set to $\alpha = 1$. Adding the logarithmic part of the tree-level contribution from $V^{(3)}_{\mathrm{EFT}}$, this leads to the logarithmic part of $\mathcal{C}_4(k_{\mathrm{F}})$ given in Eq. (16).

Finally, the infrared divergences are due to repeated energy denominators. This is a generic feature of two-particle reducible contributions in zero-temperature MBPT [26]. At each order, the infrared singularities are removed when certain two-particle reducible diagrams are combined, in the present case III(1+8) and III(2+10). The expression for III(1+7+8) is given by[1]

$$E_{4,\mathrm{III}(1+7+8)} = -\zeta(g-1)\sum_{\substack{\mathbf{i,j,k}\\\mathbf{a,c}}} n_{ijk}\bar{n}_{abc}\frac{\theta_{\mathbf{ab}}}{\mathcal{D}^2_{ab,ij}}$$

$$\times \left(\bar{n}_d\frac{\theta_{\mathbf{ka}}\theta_{\mathbf{cd}}}{\mathcal{D}_{bcd,ijk}} - \bar{n}_{d'}\frac{\theta_{\mathbf{cd'}}}{\mathcal{D}_{cd',ik}}\right)\Bigg|_{\substack{\mathbf{b=i+j-a}\\\mathbf{d=k+a-c}\\\mathbf{d'=i+k-c}}},$$
(17)

where $\zeta = k_{\mathrm{F}}^9 g(g-1)(C_0)^4$ and $\theta_{\mathbf{ab}} \equiv \theta(\Lambda/k_{\mathrm{F}} - |\mathbf{a}-\mathbf{b}|/2)$. The infrared divergence corresponds to $\mathcal{D}_{ab,ij} = 0$, and in that case the two terms in the large brackets cancel each other, and similar for III(2+10). For III(1+8) also the linear UV divergences are removed.[2] The remaining logarithmic UV divergence is given by $E_{4,\mathrm{III}(1+7+8)} \xrightarrow{\Lambda\to\infty} \zeta(g-1)\sqrt{3}/(3^3 2^7 \pi^{10})\ln(\Lambda/k_{\mathrm{F}})$. Subtracting this term from Eq. (17) enables the numerical evaluation of the regular (i.e., nonlogarithmic) contribution from III(1+7+8) to $\mathcal{C}_4(k_{\mathrm{F}})$. The evaluation of the regular contributions

———

[1] Here, $\sum_{\mathbf{i}} \equiv \int d^3 i/(2\pi)^3$, the distribution functions are $n_{ij...} \equiv n_i n_j \cdots$ and $\bar{n}_{ab...} \equiv \bar{n}_a \bar{n}_b \cdots$, with $n_i \equiv \theta(1-i)$ and $\bar{n}_a \equiv \theta(a-1)$, and the energy denominators are given by $\mathcal{D}_{ab,ij} \equiv (a^2 + b^2 - i^2 - j^2)/(2M)$. For details on the diagrammatic rules, see, e.g., Ref. [19].

[2] The counterms for the power divergences of III1 and III8 would come from diagrams with single-vertex loops.
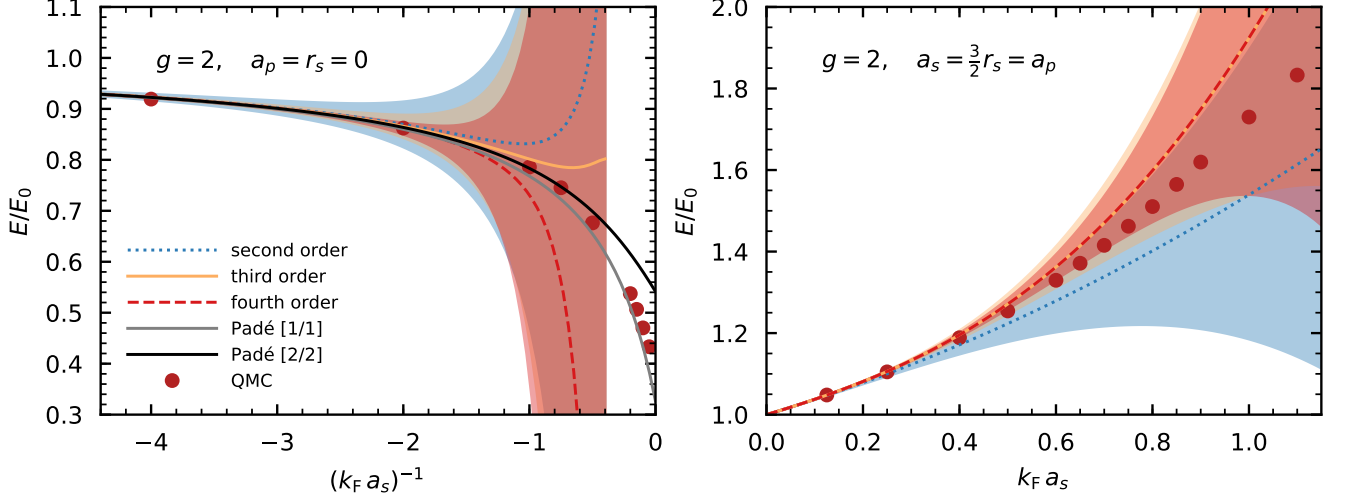
Figure 2. Results for E/E_0 from the Fermi-momentum expansion and from QMC calculations [23–25], see text for details. For clarity, in the left panel the order-by-order results are plotted only up to $k_{\rm F} a_s = -2.5$.

from II5 and IIA1 is similar, i.e., the corresponding $\ln(\Lambda/k_{\rm F})$ terms have to be subtracted.

This leaves the diagrams with power divergences II(1,2,6), where diagram II6 has also a logarithmic divergence. The expression for II6 reads

$$
E_{4,\mathrm{II6}} = -\zeta(g-3) \sum_{\substack{\mathbf{i,j,k} \\ \mathbf{a,c}}} n_{ijk} \bar{n}_{abcde} \theta_{\mathbf{ab}} \theta_{\mathbf{ka}} \theta_{\mathbf{cd}} \theta_{\mathbf{je}} \theta_{\mathbf{be}}
$$

$$
\times \left. \frac{1}{\mathcal{D}_{ab,ij} \mathcal{D}_{be,ik} \mathcal{D}_{bcd,ijk}} \right|_{\substack{\mathbf{b=i+j-a} \\ \mathbf{d=k+a-c} \\ \mathbf{e=k+a-j}}}. \quad (18)
$$

Here, $\theta_{\mathbf{ka}}$, $\theta_{\mathbf{je}}$ and $\theta_{\mathbf{be}}$ are redundant. Substituting $\mathbf{K} = (\mathbf{i}+\mathbf{j})/2$, $\mathbf{p} = (\mathbf{i}-\mathbf{j})/2$, $\mathbf{z} = \mathbf{k}$, $\mathbf{A} = (\mathbf{a}-\mathbf{b})/2$, and $\mathbf{Y} = (\mathbf{c}-\mathbf{d})/2$ leads to

$$
E_{4,\mathrm{II6}} = -8M^3 \zeta(g-3) \sum_{\substack{\mathbf{K,p,z} \\ \mathbf{A,Y}}} n_{ijk} \bar{n}_{abcde} \, \theta_A \theta_Y \, \frac{1}{A^2 - p^2}
$$

$$
\times \frac{1}{\left[(\mathbf{A}+\mathbf{p}) \cdot (\mathbf{A}-\mathbf{K}+\mathbf{z}) \right] (Y^2 - p^2 + \mathcal{R})}, \quad (19)
$$

where $\mathcal{R} = (3\mathbf{A}+\mathbf{K}-\mathbf{z}) \cdot (\mathbf{A}-\mathbf{K}+\mathbf{z})/4$ and $\theta_A \equiv \theta(\Lambda/k_{\rm F} - A)$. The two divergences of II6 can now be separated via

$$
\frac{1}{Y^2 - p^2 + \mathcal{R}} = \underbrace{\frac{1}{Y^2}}_{\sim E_{4,\mathrm{II6(i)}}} + \underbrace{\frac{p^2 - \mathcal{R}}{(Y^2 + \mathcal{R})Y^2}}_{\sim E_{4,\mathrm{II6(ii)}}}, \quad (20)
$$

with $E_{4,\mathrm{II6(i)}} \sim \Lambda$ for $\Lambda \to \infty$, and $E_{4,\mathrm{III6(ii)}} \xrightarrow{\Lambda \to \infty} \zeta(g-3)\sqrt{3}/(3^3 2^7 \pi^{10}) \ln(\Lambda/k_{\rm F})$. The evaluation of the contribution from III6(ii) is similar to III(1,7,8), II5, and IIA1. For III6(i), the effect of the counterterm can be

implemented via the identity

$$
\frac{\Lambda}{2\pi^2} - \sum_{\mathbf{Y}} \bar{n}_{cd} \frac{\theta_Y}{Y^2} \xrightarrow{\Lambda \to \infty} \sum_{\mathbf{Y}} (n_c + n_d - n_{cd}) \frac{\theta_Y}{Y^2}. \quad (21)
$$

For diagrams II(1,2) as well as I(1,2,4,5), the same procedure can be applied. For I(1,2,4,5) we have reproduced the semianalytic results in this way.

Our results for the various contributions to the regular part of $\mathcal{C}_4(k_{\rm F})$ are listed in Table 1. The numerical values for the diagrams without divergences are similar (but small differences are present) to the ones published by Baker in Table IV of Ref. [6].[3] The contributions that involve logarithmic divergences, II5, II6, IIA1, and III(1+7+8), have the largest numerical uncertainties. For $g = 2$ more precise results can be given for II5+IIA1 and II6+III(1+7+8), because then no logarithmic divergences occur.

For spin one-half fermions, the logarithmic term at fourth order (and beyond, up to a certain order $N_{\log}$) is Pauli blocked, so in that case the $k_{\rm F}$ expansion is (for $N < N_{\log}$) given by

$$
g = 2: \quad E(k_{\rm F}) = E_0 \left(1 + \sum_{\nu=1}^{N} X_\nu \delta^\nu \right) + o(\delta^N), \quad (22)
$$

where $\delta = k_{\rm F} a_s$ and $E_0 = 3n k_{\rm F}^2/(10M)$. The coefficients X_n are completely determined by the ERE parameters.

_____

[3] The expression for $\mathcal{C}_4(k_{\rm F})$ for $g = 2$ published by Baker [6] deviates from our result. In particular, it involves an additional parameter b_2 that is presumed to be "not determined by the two-body phase shifts" [5, 6]. The appearance of such a non-ERE parameter is not justified at this order (for $g = 2$), see also [5, 7].

For $r_s = a_p = 0$ (LO), the coefficients are

$$(X_1, X_2, X_3, X_4) = (+0.354, +0.186, +0.030, -0.071),\tag{23}$$

and for the hard-sphere gas (HS) with $a_s = 3r_s/2 = a_p$, we obtain

$$(X_1, X_2, X_3, X_4) = (+0.354, +0.186, +0.384, +0.001).\tag{24}$$

The results for $N \in \{2, 3, 4\}$ are plotted in Fig. 2. For comparison, we also show results obtained from quantum Monte-Carlo (QMC) calculations [23–25]. Overall, the perturbative results are very close to the QMC results for $|\delta| \lesssim 0.5$ and start to deviate strongly for $|\delta| \gtrsim 1$. In the LO case, the relative error with respect to the QMC point at $\delta = -0.5$ is 4.5% at first, 0.8% at second, 0.4% at third, and 0.1% at fourth order. In the HS case X_4 is very small and the $N = 3$ and $N = 4$ curves are almost indistinguishable.

In Fig. 2 we also plot uncertainty bands obtained by setting $X_{N+1} = \pm \max[X_{\nu \leq N}]$. Going to higher orders in that scheme reduces the width of the bands in the perturbative region $|\delta| \lesssim 1$. For $|\delta| \lesssim 0.5$ the bands are very small for $N = 4$, which supports the conclusion that the expansion is well-converged at fourth order in this regime.

Finally, for the LO case we also plot the results obtained from the Padé[1, 1] and [2, 2] approximants. Only diagonal Padé approximants have a meaningful unitary limit. The Padé[2,2] results are very close to the QMC points for $\delta \lesssim -1.2$, while the Padé[1, 1] ones are in better agreement with the QMC points close to the unitary limit $\delta \to -\infty$. The range for the normal (i.e., non-superfluid) Bertsch parameter obtained from the Padé[1, 1] and [2, 2] approximants, $\xi_n \in [0.33, 0.54]$, is consistent with the value $\xi_n = 0.45$ extracted from experiments with cold atomic gases [27]. Altogether, these results may indicate that Padé approximants converge in a larger region, compared to the Fermi-momentum expansion. To further investigate this one would need to construct the subsequent Padé[ν, ν] approximants, which require the expansion coefficients up to order $2\nu \geqslant 6$. The main challenge (apart from the large increase of the number of diagrams) herein lies in the evaluation of diagrams with logarithmic divergences.

In summary, using EFT methods we have calculated the complete fourth-order term in the Fermi-momentum expansion for the ground-state energy of a dilute Fermi gas. A detailed study of the convergence behavior and comparison against QMC calculations for the case of spin one-half fermions showed that this (asymptotic) expansion is well-converged at this order for $|k_F a_s| \lesssim 0.5$, and exhibits divergent behavior for $|k_F a_s| \gtrsim 1$. Our results provide important high-order benchmarks for many problems in many-body physics, ranging from cold atomic gases to dilute nuclear matter and neutron stars.

* E-mail: wellenhofer@theorie.ikp.physik.tu-darmstadt.de
† E-mail: cdrischler@berkeley.edu
‡ E-mail: schwenk@physik.tu-darmstadt.de

[1] T. D. Lee and C. N. Yang, Phys. Rev. 105, 1119 (1957).
[2] V. N. Efimov, Phys. Lett. 15, 49 (1965).
[3] M. Y. Amusia and V. N. Efimov, Sov. Phys. JETP 20, 388 (1965).
[4] V. N. Efimov, Sov. Phys. JETP 22, 135 (1966).
[5] M. Y. Amusia and V. N. Efimov, Ann. Phys. 47, 377 (1968).
[6] G. A. Baker, Rev. Mod. Phys. 43, 479 (1971).
[7] R. F. Bishop, Ann. Phys. 77, 106 (1973).
[8] E. H. Lieb, R. Seiringer, and J. P. Solovej, Phys. Rev. A 71, 053605 (2005).
[9] J. V. Steele, arXiv:0010066.
[10] H.-W. Hammer and R. J. Furnstahl, Nucl. Phys. A 678, 277 (2000).
[11] R. J. Furnstahl, H.-W. Hammer, and N. Tirfessa, Nucl. Phys. A 689, 846 (2001).
[12] R. J. Furnstahl and H.-W. Hammer, Phys. Lett. B 531, 203 (2002).
[13] T. Schäfer, C.-W. Kao, and S. R. Cotanch, Nucl. Phys. A 762, 82 (2005).
[14] H.-W. Hammer and S. König, Lect. Notes Phys. 936, 93 (2017).
[15] E. Braaten and H.-W. Hammer, Phys. Rep. 428, 259 (2006).
[16] N. Kaiser, Nucl. Phys. A 860, 41 (2011).
[17] N. Kaiser, Eur. Phys. J. A 53, 104 (2017).
[18] N. Kaiser, Eur. Phys. J. A 48, 148 (2012).
[19] A. Szabo and N. S. Ostlund, Modern Quantum Chemistry (Dover Publications, New York, 1982).
[20] W. Kohn and J. M. Luttinger, Phys. Rev. 118, 41 (1960).
[21] N. Muskhelishvili, Singular Integral Equations (Dover Publications, New York, 2008).
[22] C. Drischler, K. Hebeler, and A. Schwenk, arXiv:1710.08220.
[23] S. Gandolfi, A. Gezerlis, and J. Carlson, Ann. Rev. Nucl. Part. Sci. 65, 303 (2015).
[24] S. Gandolfi, private communication.
[25] S. Pilati, G. Bertaina, S. Giorgini, and M. Troyer, Phys. Rev. Lett. 105, 030405 (2010).
[26] J. Feldman, M. Salmhofer, and E. Trubowitz, J. Stat. Phys. 84, 1209 (1996).
[27] M. J. H. Ku, A. T. Sommer, L. W. Cheuk, and M. W. Zwierlein, Science 335, 563 (2012).